Highly efficient donor-acceptor hydrazone dyes-inorganic Si/TiO_2 hybrid solar cells

Abdullah G. Al-Sehemi, Ahmad Irfan, Mohrah Abdullah M. Al-Melfi

PII: S1386-1425(15)00282-6
DOI: http://dx.doi.org/10.1016/j.saa.2015.02.108
Reference: SAA 13410

To appear in: *Spectrochimica Acta Part A: Molecular and Biomolecular Spectroscopy*

Received Date: 27 December 2014
Revised Date: 16 February 2015
Accepted Date: 22 February 2015

Please cite this article as: A.G. Al-Sehemi, A. Irfan, M.A.M. Al-Melfi, Highly efficient donor-acceptor hydrazone dyes-inorganic Si/TiO_2 hybrid solar cells, *Spectrochimica Acta Part A: Molecular and Biomolecular Spectroscopy* (2015), doi: http://dx.doi.org/10.1016/j.saa.2015.02.108

Highly efficient donor-acceptor hydrazone dyes-inorganic Si/TiO_2 hybrid solar cells

Abdullah G. Al-Sehemi[a,b,c]*, Ahmad Irfan[a*], Mohrah Abdullah M. Al-Melfi[a]

[a] Department of Chemistry, Faculty of Science, King Khalid University, Abha 61413, P.O. Box 9004, Saudi Arabia

[b] Unit of Science and technology, Faculty of Science, King Khalid University, Abha 61413, P.O. Box 9004, Saudi Arabia

[c] Research Center for Advanced Materials Science, King Khalid University, P.O. Box 9004, Abha 61413, Saudi Arabia

Abstract

We have synthesized the two donor-bridge-acceptor organic dyes (hydrazone dye 1 (HD1) and hydrazone dye 2 (HD2)) with the aim to enhance intra-molecular charge transfer then characterized by FTIR and NMR. The ground state geometries have been optimized at three different levels of theories, i.e., B3LYP/6-31G*, B3LYP/6-31G** and Hartee-Fock HF/6-31G**. The absorption spectra and oscillator strengths in different solvents have been computed and compared with the experimental data. The vibrational spectral assignments have been performed on the recorded FTIR spectra based on the theoretical predicted wavenumbers at three different levels of theories. The effect of different solvents ($CHCl_3$, CH_3CN and C_2H_5OH) has been studied on the absorption wavelengths. Furthermore, we have computed the ionization potentials, electron affinities and

* Corresponding author: Ahmad Irfan
E-mail: irfaahmad@gmail.com
Tel.:0096672418632
Fax:0096672418426
A.G. Al-Sehemi
E-mail: agmasq@gmail.com

reorganization energies of studied compounds and shed light on the charge transport properties. The hetero-junction solar cell devices were fabricated by organic-inorganic hetero-junction (Si/TiO_2/dye) then the efficiency has been measured by applying the incident power 30, 50 and 70 mW/cm^2. The maximum efficiency 3.12% has been observed for HD1.

Keywords: Organic-inorganic hybrid solar cells; Hydrazones; Fabrication; Efficiency: Density functional theory

1. Introduction

The record efficiency of conventional solar cells (inorganic materials) has been reached up to 25% [1]. Nowadays, researchers are focusing to design materials and techniques to fabricate devices which have low processing cost, easy to fabricate and environmental friendly. The organic solar cells have attained efficiency up to 10% [2]. The major issue for organic solar cell materials is not only the low efficiency until now but also stability issue [3]. In recent years, dye-sensitized solar cells [4-8] and hybrid solar cells using nanoparticles like TiO_x [9], ZnO [10], CdSe [11], CdS [12], PbS [13], $CuInS_2$ [14] gained interest. The Si based hybrid solar cells have been studied intensively [15-17]. The organic-inorganic hybrid solar cells are good and efficient as both of the materials take part to enhance the efficiency [18, 19] and inorganic part which also act as acceptor is environmentally stable and excitons absorbed here [3].

With the aim to improve the efficiency of device, we have synthesized donor-bridge-acceptor efficient organic dyes, i.e., hydrazone dye 1 (HD1) and hydrazone dye 2 (HD2), see Fig. 1. We discussed the exciton binding energy and dissociation of excitons on the basis of energies of frontier molecular orbitals as well as favorable band alignment

has been discussed thoroughly. By applying the DFT approach, we shed light on the absorption and IR spectra then compared with the available experimental data. The charge transfer behavior was studied on the basis of ionization potential, electron affinity and reorganization energy. The effect of three different level of theories, i.e., B3LYP/6-31G*, B3LYP/6-31G** and HF/6-31G** has been discussed. The structures-properties relationship has been discussed. To improve efficiency we have fabricated the dye/TiO_2/Si hybrid solar cells. The paper has been divided as; first section deals with the computational and experimental methodology. In section 3.1, we discussed the charge transfer properties and chemical descriptors. The main focus of this study is detailed investigation about the fabrication techniques and efficiency measurements.

Insert Fig. 1

2. Methodology

2.1. General experimental methods

Infra-red (IR) spectra of crystalline compounds were determined using a Thermo scientific smart omni-transmission. ^{1}H and ^{13}C nuclear magnetic resonance (NMR) spectra were recorded on a Bruker at 500 MHz Ultra Shield ^{TM} at room temperature in deutrated dimethyl sulfoxide (DMSO-d_6) (CH_3SOCH_3 have two signals in ^{1}H-NMR at δ 2.52 singlet, 3.38 singlet). UV-Vis spectra were recorded with UV-1800 Shimadzu. Melting points (mps) were determined with a Stuart SMP11 without correction.

2.1.1. Physical data

For nuclear magnetic resonance (NMR) spectra, chemical shifts and expressed in ppm on the δ- scale relative to the internal standard (TMS). The following abbreviations are used s- singlet, t- triplet, q- quartet, d- doublet, m- multiplet; J is the coupling constant (Hz).

2.1.2. General procedure for hydrazones

We have synthesized the hydrazone based sensitizers by the same method as in previous studies [20, 21]. The hydrazone derivatives would be prepared through direct condensation between the corresponding aromatic aldehydes and phenyl hydrazine. Equimolar quantities of phenylhydrazine and the aldehydes would be boiled in ethanol for an hour. The precipitated hydrazones would be filtered, washed and dried. The pure hydrazones would be obtained after recrystallization from ethanol.

2.1.3. Preparation of 1-phenyl-2-(3,4,5-trimethoxybenzylidene)hydrazine (1)

The 3,4,5-trimethoxybenzaldehyde (9.8g, 0.05 mol) was added to phenylhydrazine (4.9 ml, 0.05 mol) and added 30 ml of ethanol absolute as solvent. The flask was related with condenser under reflux system and solution boiled at 170-180 ˚C for 1h then transfer solution to beaker and stilled in room temperature or cooled, the precipitated hydrazones would be collected and filtered, washed with ethanol then dried. The product crystallization from ethanol gave yellow crystals of title compound (1-phenyl-2-(3,4,5-trimethoxybenzylidene)hydrazine) m.p 125 ˚C. δ H (DMSO, 500 MHz) 6.74-7.24 (7H, m, Ar-H), 7.80 (1H, s, CH═N), 10.32 (1H, s, NH); δ C (DMSO, 500 MHz) 55.83,56.04 and 60.06 (3xOCH_3), 102.82-145.27(8C-Ar), 153.13 (CH═N).

2.1.4. Preparation of 2-ethoxy-4-((2-phenylhydrazono)methyl)phenol (2)

The 3-ethoxy-4-hydroxybenzaldehyde (8.3g, 0.05mol) was added to phenylhydrazine (4.9 ml, 0.05mol) and added 30 ml of ethanol absolute as solvent. The flask was related with condenser under reflux system and solution boiled at 170-180 ˚C for 1h then transfer solution to beaker and stilled in room temperature or cooled, the precipitated hydrazones would be collected and filtered, washed with ethanol then dried. The product

crystallization from ethanol gave crystals of title compound (2-ethoxy-4-((2-phenylhydrazono)methyl)phenol) δ H (DMSO, 500 MHz) 1.37 (3H, t, *J* 6.5-7, CH3), 4.09(2H, q, *J* 7, CH2), 6.69-7.24 (8H, m, Ar-H), 7.76 (1H, s, CH═N), 9.16(1H, s, OH), 10.07 (1H, s, NH); δ C (DMSO, 500 MHz) 14.74 (CH3), 63.82(CH2), 109.87, 111.72, 115.54, 118.14, 119.67, 127.35, 129.0, 137.27, 145.62 and 147.26 (8C-Ar), 147.39 (CH═N).

2.1.5. General procedure for dyes

The new chromospheres were prepared by direct tricyanovinylation of hydrazones. A solution of the requisite hydrazone 1 (0.01 mol) and tetracyanoethylene (TCNE) in DMF (20 mL) was stirred at 60-90 ^{o}C for 8-12h or boiled at high temperature up to 400˚C for 8h. The solvent was removed and the residual solid was collected and recrystallized from toluene/ petroleum ether mixture.

2.1.6. Preparation of 2-{4-[2-(3,4,5-trimethoxybenzylidene)hydrazine]phenyl}ethylene-1,1,2-tricarbonitrile (HD1)

The 1-phenyl-2-(3,4,5-trimethoxybenzylidene)hydrazine (1) (2.86g, 0.01 mol) was dissolved in 20 ml DMF as solvent then added 1.28g of TCNE direct gave dark color solution. The solution was boiled at 278-285˚C under reflux for 8h. The solvent was removed and the solid residual was collected and recrystallized from toluene/ petroleum ether mixture to get violet crystals of (HD1) (3.46g 89.4%) m.p 248˚C. δ H (DMSO, 500 MHz) 3.72 (3H, s, OC$\underline{H}_3$), 3.87 (6H, s, 2xO$\underline{CH}_3$), 7.1, 8.01 and 8.02 (6H, m, Ar-H), 8.06 (1H, s, C$\underline{H}$═N), 11.85 (1H, s, N$\underline{H}$ exchange with D_2O); δ C (DMSO,500 MHz) 55.99 and 60.13 (3xO$\underline{C}H_3$), 79.12 and 144.47 ($\underline{C}$═$\underline{C}$), 114.01, 114.22 and 114.83

(3xC≡N), 104.27, 113.09, 119.36, 129.73, 132.76, 137.12, 139.20 and 151.19 (8C-Ar), 153.21(CH═N).

2.1.7. Preparation of 2-{4-[2-(3-ethoxy-4-hydroxybenzylidene}hydrazino]phenyl)-ethylene-1,1,2-tricarbonitrile (HD2)

The 2-ethoxy-4-((2-phenylhydrazono)methyl)phenol (2) (2.56g, 0.01 mol) was dissolved in 20 ml DMF as solvent then added 1.28g of TCNE direct gave dark color solution. Then the solution was boiled at 210˚C under reflux for 8h. The solvent was removed and the solid residual was collected and recrystallized from toluene/ petroleum ether mixture to get violet crystals of (HD2) (3.02g 84.6%) m.p 225-227˚C. δ H (DMSO) 1.38 (3H, t, *J* 7, OCH_2CH_3), 4.1 (2H, q, *J* 6.9-7, OCH_2CH_3), 6.85-8.01 (7H, m, Ar-H), 8.04 (1H, s, CH═N), 9.54 (1H, s, OH exchange with D_2O), 11.77(1H, s, NH exchange with D_2O); δ C (DMSO) 14.68 (CH_3CH_2O), 63.92 (CH_3CH_2O), 77.59 and 145.65 (C═C), 114.25, 114.44 and 114.89 (3xC≡N), 110.61, 115.60, 119.07, 121.94,125.57, 132.85, 136.59, 147.23 and 149.35 (9C-Ar), 151.27(CH═N).

2.2. Computational details

The density functional theory (DFT) is good approach to reproduce the experimental data as well as to predict the properties of interests [5, 6, 22-24]. The B3LYP has been proved an efficient approach to reproduce the experimental data for the small molecules [25]. Moreover, by using the large fraction of HF exchange charge transfer states have been discussed previously [26]. The B3LYP functional has been applied to compute and reproduce the absorption wavelengths of different organic dyes (indigo, azobenzene, phenylamine, hydrazone, and anthraquinone) and 0.12 eV average deviation was observed for hydrazone dyes [27]. Recently, we showed that the B3LYP is

good choice to reproduce the excitation energies for hydrazone based dyes [28-30]. We found that B3LYP (Polarizable continuum model (PCM), methanol) is better, accurate and more reasonable choice than BHandHLYP, LC-BLYP and CAM-B3LYP (PCM, methanol) to reproduce the experimental data. In the present study we have computed the excitation energies by using TD-B3LYP functional. The effect of solvents ($CHCl_3$, CH_3CN and C_2H_5OH) has been studied on the absorption spectra.

Geometry optimization for all dyes have been performed using DFT at the B3LYP/6-31G*, B3LYP/6-31G** and HF/6-31G** levels of theories. The vibrational modes were examined by using the ChemCraft program. The absorption spectra and energy gap for dyes were calculated in different solvents by using polarizable continuum model (PCM) [31] at TD-B3LYP/6-31G* level of theory [32]. The ionization potentials, electron affinities and reorganization energy of all dyes have been performed by using the B3LYP/6-31G* level of theory. All of the calculations were performed by using Gaussian-09 program package [33].

3. Results and discussion

3.1. Electronic properties and absorption spectra

The computed HOMOs energies (E_{HOMO}), LUMOs energies (E_{LUMO}) and HOMO-LUMO energy gaps (E_{gap}) have been illustrated in Fig. 2. In solvents the E_{HOMO} level elevated as compared to gas phase. In $CHCl_3$, CH_3CN and C_2H_5OH the E_{HOMO} of HD1 are -0.12, -0.17 and -0.16 eV high, respectively as compared to the E_{HOMO} in gas phase. The E_{HOMO} of HD2 in $CHCl_3$, CH_3CN and C_2H_5OH are -0.14, -0.18 and -0.18 eV higher than the E_{HOMO} without solvent, respectively. The solvents have no significant effect to elevate or diminish the E_{LUMO}. The root cause of reduced E_{gap} in solvents is the elevation

of E_{HOMO}. We observed that the effect of CH_3CN and C_2H_5OH solvents on the E_{HOMO} and E_{LUMO} is similar to lift up or reduce resulting corresponding E_{gap}. The larger E_{gap} in $CHCl_3$ revealing that all the studied dyes would be red shifted in CH_3CN and C_2H_5OH.

Insert Fig. 2

The HOMO and LUMO energies of Si are –5.43 and -3.92 eV [34, 35]. The HOMO and LUMO energies of TiO_2 are –7.40 and -4.20 eV [36]. We have observed the Nested band alignment in the donor and acceptor frontier molecular orbitals by considering the Si as acceptor only. The successful operation of a photovoltaic device requires a staggered band alignment heterojunction which allocate electrons to transport to the cathode and holes to the anode. By considering the average values both for Si and TiO_2, the valance band energy has been found -6.41 eV while the conduction band energy -4.06 eV (Si/TiO_2). It is expected that Si/TiO_2 acceptor changed the alignment to staggered band alignment heterojunction, see Fig. 2.

In hybrid solar cells, excitons formed in the donor material are dissociated at the donor–acceptor (D–A) interface. The force required to overcome the exciton binding energy is provided by the energy level offset of the lowest unoccupied molecular orbital (LUMO) of the donor and the conduction band edge of the acceptor materials. We found energy level offset 0.74 and 0.83 eV for HD1 and HD2, respectively to overcome the exciton binding energy. In HD1 less force is required to overcome the exciton binding energy as compared to other dye. For dissociation of excitons formed in the acceptor material, the energy offset of the highest occupied molecular orbital (HOMO) of the donor and the valence band edge of the acceptor materials is required. We found energy

level offset 0.57 and 0.68 eV for HD1 and HD2, respectively to dissociate of excitons. In HD1 less force would be required for dissociation of excitons. It is expected that HD1 would be more efficient because of less force would be required to overcome the exciton binding energy as well as dissociation of excitons.

Insert Table 1

In HD1 the maximum absorption wavelength has been observed at 529 nm in chloroform and 532 nm in acetonitrile, no significant effect has been observed in absorption spectra toward red shift by changing chloroform to CH_3CN. In HD2 substitution of *m*-OC_2H_5, *p*-OH showed absorption band at 538 nm in chloroform, 543 nm in CH_3CN and 547 nm in ethanol.

The dyes were measured in various solvents having different polarity, see Table 1. The trend of absorption spectra toward red shift of HD1 and HD2 in different solvents is $CHCl_3$ < CH_3CN < CH_3CH_2OH. The maximum absorption spectra computed at TD-B3LYP/6-31G* level of theory in chloroform is 568 and 587 nm for HD1 and HD2, respectively. The maximum absorption wavelengths in acetonitrile are 570 and 593 nm for HD1 and HD2, respectively. In ethanol, we observed the maximum absorption wavelength at 570 and 593 nm for HD1 and HD2, respectively which are in reasonable agreement with the experimental evidence.

3.2. FTIR spectra

Vibrational spectral assignments were recorded based on the theoretical predicted wavenumbers by DFT/B3LYP/6-31G*, B3LYP/6-31G** and HF/6-31G** level of

theories. ChemCraft graphical interface was used to assign the calculated harmonic wavenumbers using scaled displacement vectors to identify the motion of modes. The computed wavenumbers by DFT are in good agreement with the experimental values, see Fig. 3. The IR spectra calculated were made for a free molecule in vacuum while experiments were performed for solid sample. For this reason we used scale factors in theoretical method. In this study, we have used the scaling factor 0.937 for investigated dyes except HD2 (0.930) for DFT calculations and 0.866 and 0.845 scaling factor for HD1 and HD2, respectively for HF calculations.

The FTIR spectra exhibited three important absorption bands; the first band has been observed at 3271 and 3250 cm^{-1} for the (ν_{N-H}) mode for HD1 and HD2, respectively. In the present case DFT calculations gave 3382 and 3349 cm^{-1} at B3LYP/6-31G* and 3399 and 3367 cm^{-1} at B3LYP/6-31G** while the HF calculations gave 3319 and 3239 cm^{-1} for HD1 and HD2, respectively. The NH stretching wavenumber is red shifted in IR from the computed wavenumber, which indicates the weakening of the N—H bond resulting in hydrogen bonding. The strong and sharp second band appears in the region of 2219-2215 which was attributed to the cyano group. The B3LYP/6-31G* and B3LYP/6-31G** calculations gave these modes at 2200 and 2183 cm^{-1} while HF calculations gave at 2265 and 2210 cm^{-1} for HD1 and HD2, respectively. The third absorption band in the region of 1610 and 1608 cm^{-1} ascribed for the C═N in HD1 and HD2, respectively. The DFT calculations gave at 1574 and 1564 cm^{-1} at B3LYP/6-31G* level of theory and 1570 and 1561 cm^{-1} at B3LYP/6-31G** level of theory while the HF calculations gave at 1656 and 1617 cm^{-1} for HD1 and HD2, respectively. The absorption of OH group appear in HD2 in the range 3143–3443 cm^{-1} (FTIR), from 3139 to 3577 cm^{-1} for DFT and from

3261 to 3564 cm^{-1} for HF. The N-H stretching vibration showed only one band at 3335 cm^{-1} [37]. The sharp band has been observed at 3265 cm^{-1} in the FTIR spectrum for the title compounds. The DFT calculations gave 3361 and 3379 cm^{-1} for B3LYP6-31G* and B3LYP6-31G**, respectively. The HF calculations gave band at 3462 cm^{-1}. Effect of hydrogen bonding on an O–H stretching vibration appeared in the region (3500–2500) cm^{-1} [37]. The υ_{O-H} mode is interference with N─H stretching mode and seen broad band in the region about 3143 cm^{-1}. In DFT calculations gave 3139 and 3152 cm^{-1} for B3LYP/6-31G* and B3LYP/6-31G** level of theories, respectively. The HF calculations gave at 3261 cm^{-1}.

For the existence of benzene rings in a structure, the C─H and C═C─C vibrations is varying and depending on the number and type of substitutions. In case of disubstituted on benzene ring, the υ_{C-H} symmetric and asymmetric showed in region (3080-3030) cm^{-1} and DFT calculations gave the ν_{C-H} modes in the range 3060-2894 cm^{-1}. In the present case, the DFT calculations gave the ν_{C-H} modes in the range 3055-2982 cm^{-1} at B3LYP/6-31G* and in the range 3049-2979 cm^{-1} at B3LYP/6-31G** level of theories. In HF calculations showed bands in the range 2909-2837 cm^{-1}. For C═C─C stretching in aromatic rings are different in case 1,2-disubstituted from 1,4-disubstituted on benzene ring, the C═C stretching vibration showed in the region (1577±4) cm^{-1} and (1579±6) cm^{-1}. In the present case, the $\upsilon_{C=C}$ mode of aromatic rings occurs at 1656 cm^{-1} in IR spectra. The $\upsilon_{C=C}$ mode appeared at 1576 and 1573 at B3LYP/6-31G* and B3LYP/6-31G** level of theory, respectively. The HF calculations gave 1620 cm^{-1} for 1,2-disubstituted ring but for 1,4-disubstituted the $\upsilon_{C=C}$ mode of aromatic rings has been obsered at 1560, 1558 and 1531 cm^{-1} for B3LYP/6-31G* , B3LYP/6-31G** and HF level of theories, respectively.

The $\upsilon_{C=N}$ mode has been reported in the range (1605-1665) cm^{-1} by A. M. Asiri *et al* [38]. In present case the strong band has been observed at 1601 cm^{-1} in the FTIR spectra (C═N stretching mode). The DFT calculations gave same mode at 1570 and 1566 cm^{-1} at B3LYP/6-31G* and B3LYP/6-31G** level of theories, respectively. In HF calculations this mode has been observed at 1549 cm^{-1}. The C≡N stretching vibration has been reported in the range 2235-2215 cm^{-1}. The sharp and strong band for $\upsilon_{C\equiv N}$ mode appeared 2219 cm^{-1} in FTIR spectra. The DFT calculations gave $\upsilon_{C\equiv N}$ mode in the range 2178-2201 cm^{-1} at B3LYP/6-31G* and B3LYP/6-31G** while HF calculations gave in the range 2217-2224 cm^{-1}. The C─O stretching mode reported in literature in the range 1000-1300 cm^{-1}. In title compounds, the υ_{C-O} mode observed at 1294 cm^{-1} in FTIR while calculations showed at 1250 and 1206 cm^{-1} for DFT and HF, respectively. The C=C in aromatic rings show at 1598, 1588, 1494, and 1456 cm^{-1} [39]. The computed modes at different level of theories have been tabulated in Tables S1-S4 (Detail can be found in supporting information).

Insert Fig. 3

3.3. Chemical descriptors

The vertical ionization potentials (IPv), adiabatic ionization potentials (IPa), vertical electron affinities (EAv), adiabatic electron affinities (EAa), hole reorganization energies λ(h) and electron reorganization energies λ(e) have been tabulated in Table 2. Previously, it was concluded that higher EAv would be favorable for the generation of free [40]. The better hole transfer materials have smaller value of ionization potentials [41] while better electron transfer materials have higher electron affinities. The high EA

of HD1 is revealing that it would be more appropriate to generate free electrons and holes. The calculated hole reorganization energy of HD2 is smaller than the electron reorganization energies revealing that this dye might be better hole transport material.

Insert Table 2

The electronegativity (χ), hardness (η), electrophilicity (ω), softness (S) and electrophilicity index (ωi) at the B3LYP/6-31G*, B3LYP/6-31G**, and HF/6-31G** level of theories have been presented in Tables S5. It has been observed that the trend of the electronegativity (χ), hardness (η), electrophilicity (ω), softness (S) and electrophilicity index (ωi) at all the level of theories is similar. The χ and ω are larger for HD1. The significant effect to reduce the ωi has been observed in HD1 while reverting effect has been observed in HD2 in which strong activating group ethoxy has been substituent.

3.4. Fabrication

The Si wafer was immersed for ten seconds in HF solution (water/HF 49%) for etching purpose. Then it was rinsed in a mixture of ethanol, acetone and de-ionized water with molar ratios 1:1:3, respectively to eliminate the fluoride ions. The substrates were rinsed with dry nitrogen gas. Recently we showed that the nanoporous TiO_2 prepared by sol-gel method from the mixture of H_2O_2 and HNO_3 has better porosity about 32% and showed only pure anatase phase with energy gap of 3.2 eV. The the sol-gel solution was used to deposit a titanium oxide films on glass and silicon substrates by spin-coating method. All films were prepared at spin-coated at rate 2000 rpm (revolution per minute)

for 1 min. On pre-cleaned substrates (glass and SiO_2 etched- silicon), then dried in oven (60 oC for 10 min) and repeated pervious steps for 3 layers of coating. For building solar cell device; about 20 nm nanoporous TiO_2 film has been deposited on SiO_2 etched-Si substrate. Then about 400 nm of dye was deposited on the top of TiO_2 film. Gold is used as a top metal electrode by use of a suitable mask to control the shape of the electrode.

The dye thin films were prepared by conventional thermal evaporation technique at a pressure of about 10-6 mbar. The powder was loaded into a molybdenum cell with nozzle of 2 mm in diameter on the top. The flat glass; glass coated-TiO_2; and silicon substrates were located above 20 cm from the dye. The film thicknesses were controlled by using a quartz crystal thickness monitor and subsequently confirmed by ellipsometry measurements. The films were deposited at room temperature and the rate of deposition was 0.2nm/s. The low deposition rate was adjusted for better film quality and crystallinity [42]. The dye layer was prepared by thermal evaporation on the etched surface of Si substrate. Before depositing of the dye, a thin layer of nanoporous TiO_2 (20 nm) was deposited by sol-gel method.

3.5. Efficiency

Fig. 4 showed the current-voltage characteristics curves with open-circuit voltage and short-circuit current under different illumination power, i.e., 30, 50 and 70 mW/Cm^2. The photovoltaic properties of heterojunction organic-inorganic hybrid solar cells (Si/TiO_2/dye) based on HD1 and HD2 have been shown in Table 3. The power conversion efficiency of HD1 has been observed 2.87 with J_{sc} 2.41 mA/cm^2, V_{oc} of 570 mV and FF of 63% when the P_{in} was 30 mW/cm^2. By changing the P_{in} to 50 mW/cm^2 the HD1 gave J_{sc} 3.95 mA/cm^2, V_{oc} of 615 mV and FF of 64.20% with efficiency 3.12%. For

HD1, 2.71% efficiency has been examined when P_{in} was 70 mW/cm^2 which boosts up the J_{sc} 4.92 mA/cm^2, V_{oc} of 636 mV and FF of 61%. The power conversion efficiency 1.70% has been measured for HD2 with P_{in} 30 mW/cm^2 and J_{sc} 1.51 mA/cm^2, V_{oc} of 502 mV and FF of 67.21%. The HD2 gave J_{sc} 2.66 mA/cm^2, V_{oc} of 533 mV and FF of 64.14% with improved efficiency 1.82% when P_{in} was 50 mW/cm^2. The HD2 gave J_{sc} 4.93 mA/cm^2, V_{oc} of 592 mV and FF of 46.26% with P_{in} 70 mW/Cm^2 which improved the efficiency to 1.93%. It can be noticed that by increasing the P_{in} from 30 mW/cm^2 to 50 mW/Cm^2 J_{sc}, V_{oc} and FF improved resulting enhanced the efficiency, see Table 3.

Insert Fig. 4 and Table 3

Conclusions

The following conclusions have been drawn by our dual approach investigations:

1- Elevation of E_{HOMOs} reduces the E_{gap} in solvents while E_{LUMOs} have no significant effect to elevate or diminish it. The average values of E_{HOMOs} and E_{LUMOs} for Si/TiO_2 and donor dye showed the staggered band alignment.

2- The energy level offset values revealed that HD1 would be more efficient because less force would be required to overcome the exciton binding energy and dissociation of excitons.

3- The computed absorption wavelengths and vibrational spectral modes are in good agreement with the experimental data.

4- The high EA of HD1 is revealing that it would be more appropriate to generate free electrons and holes.

5- The direct correlation between the adiabatic electron affinity/ionization potential and the V_{oc} has been observed.

6- The HD1 showed good efficiency which reached to the 3.12%. To further increase the efficiency different metal oxides are under synthetic process in this regards which would be investigated in near future.

Acknowledgement

Mohrah Abdullah M. Al-Melfi thanks King Abdul Aziz city of Science and technology (KACST) for their financial support by the grant No. GSP-28-33.

Electronic supplementary material

The online version of this article (doi:-------) contains supplementary material.

References

[1] M.A. Green, K. Emery, Y. Hishikawa, W. Warta, E.D. Dunlop, Progress in Photovoltaics: Research and Applications, 20 (2012) 12-20.
[2] M.A. Green, Progress in Photovoltaics: Research and Applications, 9 (2001) 123-135.
[3] S. Ren, L.-Y. Chang, S.-K. Lim, J. Zhao, M. Smith, N. Zhao, V. Bulović, M. Bawendi, S. Gradečak, Nano Lett., 11 (2011) 3998-4002.
[4] A. Irfan, A.G. Al-Sehemi, S. Muhammad, Synth. Met., 190 (2014) 27-33.
[5] A. Irfan, H. Aftab, A.G. Al-Sehemi, J. Saudi. Chem. Soc., 18 (2014) 914-919.
[6] A. Irfan, R. Jin, A.G. Al-Sehemi, A.M. Asiri, Spectrochimica Acta Part A: Molecular and Biomolecular Spectroscopy, 110 (2013) 60-66.
[7] A. Irfan, N. Hina, A. Al-Sehemi, A. Asiri, J. Mol. Model., 18 (2012) 4199-4207.
[8] D. Gebeyehu, C.J. Brabec, N.S. Sariciftci, D. Vangeneugden, R. Kiebooms, D. Vanderzande, F. Kienberger, H. Schindler, Synth. Met., 125 (2001) 279-287.
[9] P.A. van Hal, M.M. Wienk, J.M. Kroon, W.J.H. Verhees, L.H. Slooff, W.J.H. van Gennip, P. Jonkheijm, R.A.J. Janssen, Adv. Mater., 15 (2003) 118-121.
[10] W.J.E. Beek, M.M. Wienk, R.A.J. Janssen, Adv. Funct. Mater., 16 (2006) 1112-1116.
[11] A.P. Alivisatos, Science, 271 (1996) 933-937.
[12] N.C. Greenham, X. Peng, A.P. Alivisatos, Phys. Rev. B, 54 (1996) 17628-17637.
[13] S.A. McDonald, G. Konstantatos, S. Zhang, P.W. Cyr, E.J.D. Klem, L. Levina, E.H. Sargent, Nat Mater, 4 (2005) 138-142.
[14] E. Arici, N.S. Sariciftci, D. Meissner, Adv. Funct. Mater., 13 (2003) 165-171.
[15] A.G. Al-Sehemi, A. Irfan, M.A.M. Al-Melfi, A.A. Al-Ghamdi, E. Shalaan, J. Photochem. Photobiol., A: Chem., 292 (2014) 1-9.
[16] M. Wright, A. Uddin, Sol. Energy Mater. Sol. Cells, 107 (2012) 87-111.
[17] S.-H. Tsai, H.-C. Chang, H.-H. Wang, S.-Y. Chen, C.-A. Lin, S.-A. Chen, Y.-L. Chueh, J.-H. He, ACS Nano, 5 (2011) 9501-9510.
[18] T. Xu, Q. Qiao, Energy Environ. Sci., 4 (2011) 2700-2720.
[19] Y. Zhou, M. Eck, M. Kruger, Energy Environ. Sci., 3 (2010) 1851-1864.

[20] A.G. Al-Sehemi, A. Irfan, A.M. Asiri, Y.A. Ammar, Spectrochimica Acta Part A: Molecular and Biomolecular Spectroscopy, 91 (2012) 239-243.
[21] A.G. Al-Sehemi, A. Irfan, A.M. Asiri, Y.A. Ammar, J. Mol. Struct., 1019 (2012) 130-134.
[22] A. Irfan, A.G. Al-Sehemi, S. Muhammad, Journal of Quantum Chemistry, 2014 (2014) 6.
[23] A. Irfan, A.G. Al-Sehemi, J. Saudi. Chem. Soc., 18 (2014) 574-580.
[24] A. Irfan, A.G. Al-Sehemi, M.S. Al-Assiri, J. Mol. Graphics Modell., 44 (2013) 168-176.
[25] B.M. Wong, J.G. Cordaro, J. Chem. Phys., 129 (2008) -.
[26] R.J. Magyar, S. Tretiak, Journal of Chemical Theory and Computation, 3 (2007) 976-987.
[27] D. Guillaumont, S. Nakamura, Dyes Pigm., 46 (2000) 85-92.
[28] A. Al-Sehemi, M. Al-Melfi, A. Irfan, Struct. Chem., 24 (2013) 499-506.
[29] A. Al-Sehemi, A. Irfan, A. Asiri, Theor. Chem. Acc., 131 (2012) 1199-1208.
[30] A.G. Al-Sehemi, A. Irfan, A.M. Asiri, Y.A. Ammar, J. Mol. Struct., (2012).
[31] C. Amovilli, V. Barone, R. Cammi, E. Cancès, M. Cossi, B. Mennucci, C.S. Pomelli, J. Tomasi, Recent Advances in the Description of Solvent Effects with the Polarizable Continuum Model, in: L. Per-Olov (Ed.) Adv. Quantum Chem., Academic Press, 1998, pp. 227-261.
[32] C. Zhang, W. Liang, H. Chen, Y. Chen, Z. Wei, Y. Wu, J. Mol. Struct. (TheoChem), 862 (2008) 98-104.
[33] M. J. Frisch et al., Inc., Wallingford, CT, (2009).
[34] C.-Y. Liu, Z.C. Holman, U.R. Kortshagen, Nano Lett., 9 (2008) 449-452.
[35] C.-Y. Liu, Z.C. Holman, U.R. Kortshagen, Adv. Funct. Mater., 20 (2010) 2157-2164.
[36] C.Y. Kuo, W.C. Tang, C. Gau, T.F. Guo, D.Z. Jeng, Appl. Phys. Lett., 93 (2008) 033307-033303.
[37] B.H. Stuart, Infrared Spectroscopy: Fundamentals and Applications, Wiley, 2004.
[38] A.M. Asiri, A.A. Bahajaj, I.M.I. Ismail, N.A. Fatani, Dyes Pigm., 71 (2006) 103-108.
[39] R. Aich, F. Tran-Van, F. Goubard, L. Beouch, A. Michaleviciute, J.V. Grazulevicius, B. Ratier, C. Chevrot, Thin Solid Films, 516 (2008) 7260-7265.
[40] L. Sun, F.-Q. Bai, Z.-X. Zhao, B.-Z. Yang, H.-X. Zhang, J. Polym. Sci., Part B: Polym. Phys., 48 (2010) 2099-2107.
[41] R.K. Chan, S.C. Liao, Can. J. Chem., 48 (1970) 299-305.
[42] L.B. Freund, Suresh, S., , Thin film materials: Stress, Defect formation and surface evolution, in, Cambridge University Press, Cambridge University Press, 2009.

Figure Captions

Fig. 1. The synthesized organic dyes HD1 and HD2.

Fig. 2. The HOMOs energies, LUMOs energies and energy gap of Dyes in different solvents (top) and gas phase (bottom) (in eV).

Fig. 3. The FTIR spectra of the studied compounds.

Fig. 4. The current-voltage characteristics curves with open-circuit voltage and short-circuit current under different illumination power, HD1 (left) and HD2 (right).

Table 1

Calculated (calc) and experimental (exp) absorption spectra (nm) and oscillator strength (f) in different solvents.

calc	CHCl3				CH3CN				EtOH			
	Exp		calc		exp		calc		exp		calc	
	λ	(f)	λ	(f)	λ	(f)	λ	(f)	λ	(f)	λ	(f)
HD1	529	0.47	568	0.71	532	1.01	570	0.71	540	1.06	570	0.71
	333	0.12	418	0.18	330	0.22	419	0.17	332	0.2	419	0.17
	288	0.02			285	0.02			288	0.03		
HD2	538	0.44	587	0.6	543	0.56	593	0.58	547	0.52	593	0.58
	340	0.05	383	0.04	338	0.09	388	0.05	342	0.11	455	0.32
	288	0.01			288	0.01			293	0.01	388	0.05

Table 2

The vertical and adiabatic ionization potentials (IPv/a), vertical and adiabatic electronic affinities (EAv/a), hole and electron reorganization energies (λh/e) of hydrazone dyes (in eV) at the B3LYP/6-31G* level.

Dyes	IPv	IPa	EAv	EAa	λh	λe
HD1	6.70	7.09	2.14	1.87	0.778	0.523
HD2	6.78	7.01	2.08	1.77	0.460	0.593

Table 3

The organic-inorganic hybrid solar cell device performance parameters.

Complexes	*Incident power* (mW/cm^2)	*Voc* (*V*)	*Jsc* (mA/cm^2)	*FF*	*Efficiency* (%)
HD1	30	0.57	2.41	0.63	2.87
	50	0.62	3.95	0.64	3.12
	70	0.64	4.92	0.61	2.71
HD2	30	0.50	1.51	0.67	1.70
	50	0.53	2.66	0.65	1.82
	70	0.59	4.93	0.46	1.93

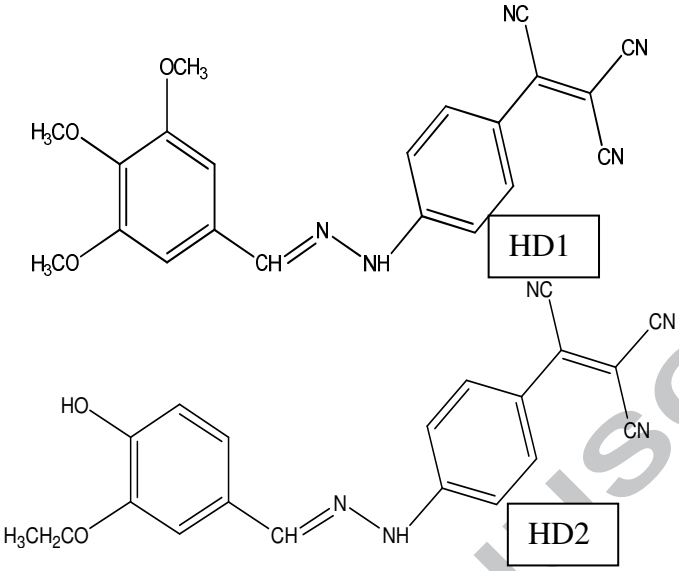

Fig. 1.

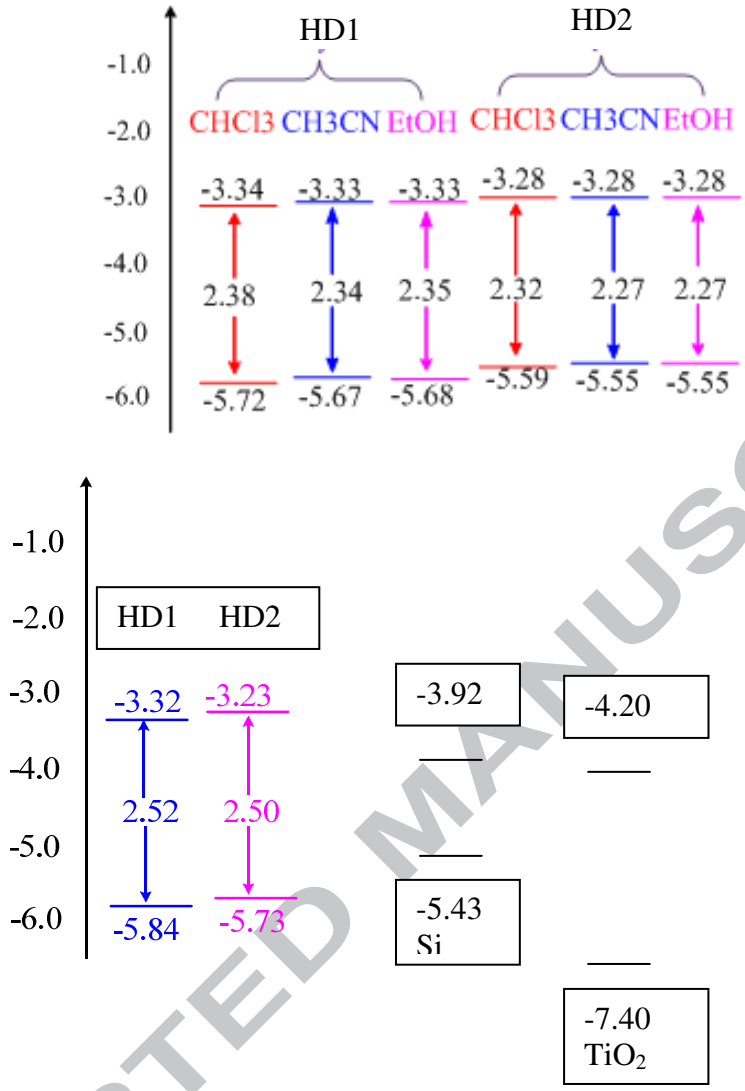

Fig. 2.

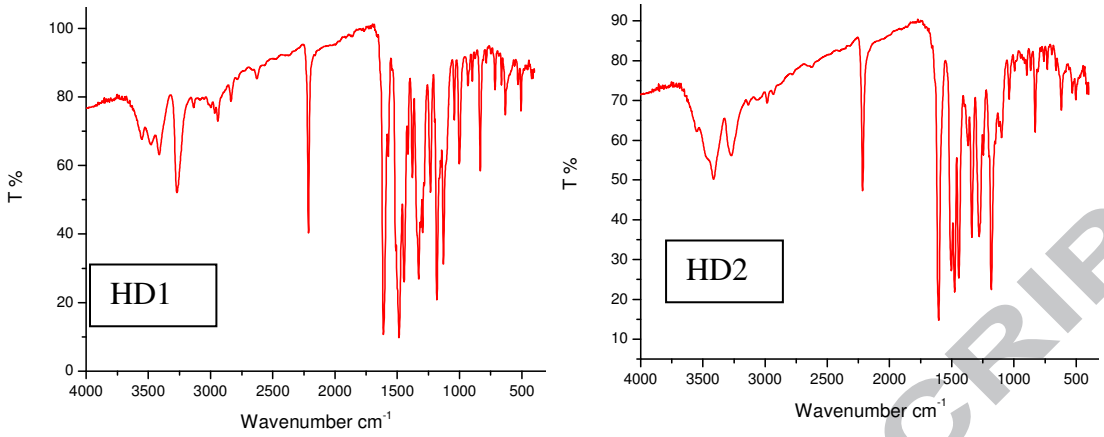

Fig. 3.

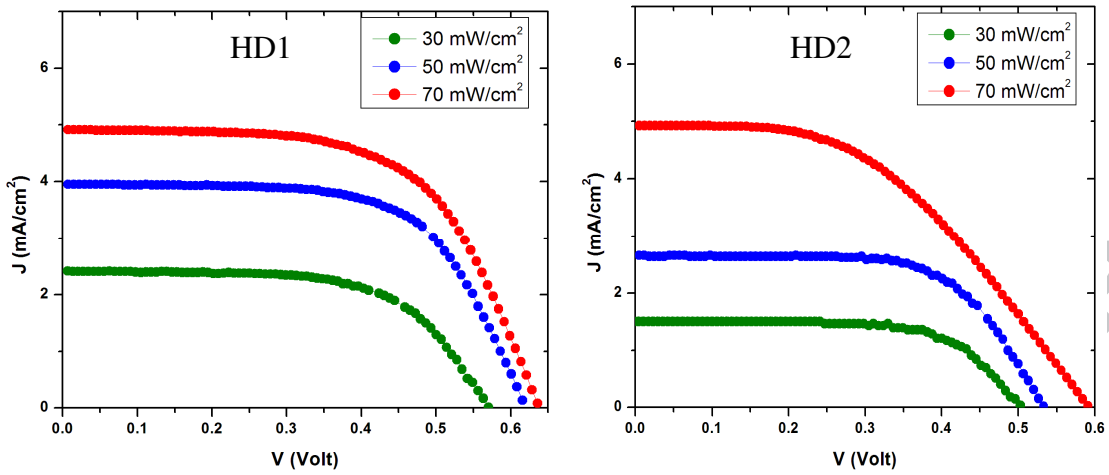

Fig. 4.

Research highlights

- D-bridge-A hydrazone dyes were synthesized and characterized by UV-Vis, FTIR, and NMR techniques.
- The effect of different solvents has been studied on the absorption wavelengths.
- Computed absorption and IR spectra are in good agreement with the experimental data.
- Direct correlation between IPa/EAa and V_{oc} has been observed.
- Hetero-junction solar cell devices were fabricated and 3.12% efficiency has been observed for HD1.